LOCAL DEFORMATION PROPERTIES OF SEGREGATED SAND SPECIMEN IN HOLLOW CYLINDRICAL TORSIONAL SHEAR TESTS

Usama Juniansyah FAUZI[1], Junichi KOSEKI[2]

ABSTRACT: A hollow cylindrical torsional shear apparatus with a special image analysis technique is employed for understanding the deformation of segregated specimen that is reconstituted by depositing Katori sand particles in three layers through water sedimentation. This specimen preparation is used to model reclaimed land constructed by dredging and pumping method. This technique involves the use of a latex membrane with dots marked in a grid pattern with approximately 5 mm spacing. These dots are tracked using a digital camera that synchronously shoots the membrane surface at desired time intervals. Corrections of coordinates are applied for the effects of cylindrical shape of specimen, the camera lenses, and refraction from lighting through water in the cell. It was observed that in drained monotonic loading test, formation of shear band was initiated at interface layers before the shear stress reached its peak value. In undrained cyclic loading test, the specimen deformation did not start uniformly but started gradually.

Key words: local deformation, water sedimentation, segregation, Katori sand, and hollow cylindrical torsional shear.

INTRODUCTION

Liquefaction causes large deformation of ground particularly consisting of sandy soils. Damage caused by liquefaction is so vast that repairing of structures on liquefied ground is difficult and costly. In most of past large earthquakes, liquefaction took place in reclaimed lands constructed by dredging and pumping method. Dredging in this paper is defined as removal of materials from the bottom of rivers or sea. The materials removed during dredging are pumped in to form reclaimed land. Under this condition, there is no soil densification performed and soil particles sediment due to gravity.

Numerous researches (Tatsuoka et al. 1986; Miura and Toki, 1982; Wood et.al., 2008; among others) have reported that the strength and deformation of sands can be remarkably influenced by methods of specimen preparation. Most prior studies have focused their efforts to establish a standard method of specimen preparation by which homogenous specimens can be formed in order to obtain reliable and repeatable results. However, these techniques may not be valid in all situations, especially when dealing with sandy soil that is deposited in-situ using the dredging and pumping method. These sandy soil deposits are not uniform where the sands and fines are segregated with beddings of millimeters to centimeters in thickness.

Yoshimine and Koike (2005) have examined the effect of micro-layer on silty sand behavior by stratified soil of five layers of clean sand and kaolin silt in triaxial apparatus. Their test results indicate that the liquefaction resistance of layered soil is greater than that of uniform sand. However, triaxial apparatus has a drawback in the sense that the shear stress generated by cyclic loading in vertical direction is not applied on the horizontal plane along which the segregated layer is formed. Kokusho et

[1] Graduate Student, Department of Civil Engineering, The University of Tokyo
[2] Professor, Institute of Industrial Science, The University of Tokyo

al. (1998) and Kokusho (2000) reported, based on model tests, soil element tests and site investigations, that the effect of soil layering on the emergence of water film, or in water interlayer term (Seed, 1987) at the interface between the top of the saturated sand strata and the base of a layer of low-permeability fines during liquefaction. The water film may play an important role in post-earthquake large lateral flow in liquefied ground. Brennan and Madabhushi (2005) gave an evidence supporting the theory of water film formation by conducting several centrifuge tests on liquefiable sand layer with thin surface fine layers and combination of vertical drain.

This paper is aimed to study the detailed liquefaction behavior of segregated specimens including property of the local deformation using hollow cylindrical torsional shear tests. Unlike the tests conducted in triaxial condition, the hollow cylindrical torsional shear test can simulate the simple shear condition in an approximated manner. Katori sand that was retrieved from a reclaimed land in Katori city, Chiba prefecture, Japan is selected for the present test because this reclaimed land suffered extensive liquefaction in March 2011 East Japan Great Earthquake Disaster. In view of the above, image analysis technique is introduced to improve measurement of specimen local deformation.

EXPERIMENT PROCEDURES

A disturbed sand sample for experiment is retrieved from a reclaimed area in Katori city, which is located near Tone River. All tests in this experimental program are performed on Katori sand with cut-off diameter of 4.75 mm, mean grain size (D_{50}) = 0.16 mm, coefficient of uniformity = 1.81, coefficient of gradation = 0.97, G_s = 2.65, maximum void ratio = 1.35, minimum void ratio = 0.92, and fines content of about 5%. Its grain size distribution curve is shown in Fig. 1.

The specimen is prepared initially by filling the specimen mold with distilled water. Specimens are prepared at Dr = 18-22% (before consolidation). We used an acrylic pipe with length of 100 cm to elongate the height of mould for specimen preparation. The planed height of soil sample is 30 cm with 3 layers. Initial water height is 50 cm. A mixture of soil and water at a mass ratio of 1:2 is used to make soil slurry (Fig. 2).

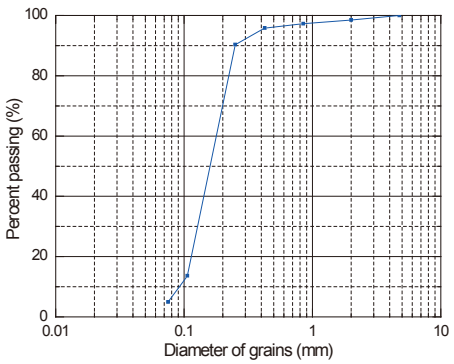

Fig. 1: Grain size distribution curves of Katori sand

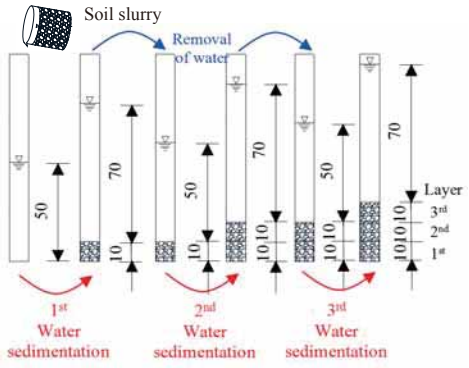

Figure 2. Illustration of sample preparation

The procedure of specimen preparation for this test was recently developed by Fauzi and Koseki (2013); by depositing Katori sand particles in the acrylic pipe through water sedimentation. A typical segregated condition is shown in Fig. 3. This special method is developed to model the reclaimed soil deposits that are constructed by dredging and pumping method. In reality, dredging and pumping method would result in segregation because of the fine particles lagging behind due to their smaller sedimentation velocities in water. As a result, the reclaimed soil deposits may not be uniform.

Sieving analyses were conducted on a part of the specimen with a thickness of 1 cm on bottom, top, and next top in each layer. The result is shown in Fig. 4, where the top zone exhibited higher silt content than the next top zone; and the next top zone exhibited higher silt content than the bottom zone.

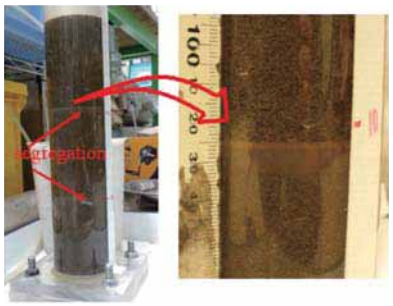

Fig. 3: Segregation observed on acrylic pipe

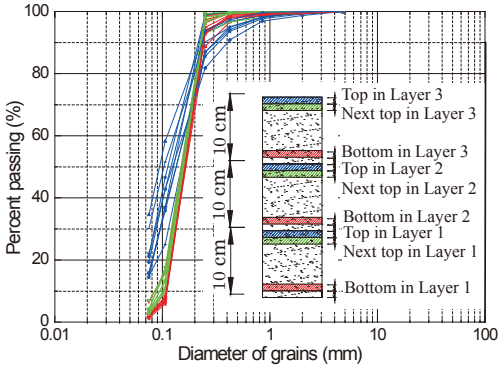

Fig. 4: Local grain size distributions of specimen with water sedimentation

Torsional shear was conducted on hollow cylindrical specimens having the height of 30 cm, the inner and outer diameters of 12 cm and 20 cm, respectively. Specimens are prepared at *Dr* = 18-22%. The top part of silt layer in layer 3 is cut so that the specimen consists of sand layers and two silt layers. Double vacuum method was used during the saturation process due to large specimen size and *B-value* could be achieved to be greater than 0.96. The specimen was consolidated isotropically to 100 kPa. Loading was performed in two cases. In the first case, drained monotonic loading was applied with constant shear strain rate of 0.5 %/min., while maintaining the other stress conditions at $\sigma_z' = \sigma_r' = \sigma_\theta' = 100$ kPa. Loading process is terminated when the shear strain exceeded 20%. In the second case, undrained cyclic loadings were applied with constant shear strain rate of 1%/min with single amplitude shear stress of 10 kPa, 15 kPa, and 20 kPa (i.e., the cyclic shear stress ratio, CSR, of 0.10, 0.15, and 0.20) while maintaining the specimen height constant.

IMAGE ANALYSIS AND STRAIN CALCULATION

Several experimental studies that focused on localized deformation have used advanced tools, e.g. stereophotogrammetry (e.g. Desrues et al., 1985, Harris et al., 1995 and Desrues et al., 2004), X-ray computed tomography (e.g. Desrues et al., 1996), image analysis techniques (e.g. Yoshida et al., 1994, Alshibli et al., 1999, Lin and Panumadu, 2006), and digital correlation techniques (Sutton et al., 1983, Reschemacher, 2003) among others. In this study, image analyses techniques by dots tracking are used. Dots with spacing of 5 mm x 5 mm grid are pasted on the outer membrane. A digital camera with the resolution of 7360 x 4912 pixels (Nikon D8000) and lighting sources are employed to observe the dots movement during the loading process as shown in Fig. 5. Each picture was captured for a prescribed interval time of 1 minute and 0.25 minutes for drained monotonic loading test and undrained cyclic loading test, respectively. These dots on the specimen were tracked in term of their center of mass using an image processing software (Move-tr/2D Ver. 7.21) with the accuracy of about 0.01 mm. By comparing image data at two different time intervals, the displacement of each dot during that time interval was obtained.

Geometric correction was performed on the pictures to cancel the distortion of an image. The distortion is caused by cylindrical shape of the specimen where three-dimensional objects are transformed into two-dimensional image as illustrated in Figure 6. In addition, the refraction of lighting through water, and lens effect of both the camera and the cell plexy glass, can magnify or reduce the size of the target. Therefore, corrections were needed to apply for determining true specimen dimensions and dot point positions.

Wahyudi et al. (2011) proposed a correction method for shear band observation study in hollow cylinder torsional apparatus. A similiar method was applied in this study. The coordinates are corrected by fitting the dots in apparent coordinate with parabola function. Then, the real coordinates are determined by transforming the measured parabolas into straight line (Fig. 6). The horizontal

coordinates are represented by

$$x_i = a_{0i} + a_{1i}.u + a_{2i}.v + a_{3i}.u^2 + a_{4i}.u.v + a_{5i}.v^2 \quad (1)$$

and the vertical by

$$y_j = b_{0j} + b_{1j}.u + b_{2j}.v + b_{3j}.u^2 + b_{4j}.u.v + b_{5j}.v^2 \quad (2)$$

where u and x are the apparent and real coordinates, respectively, in horizontal gridline, v and y are the apparent and real coordinates in vertical gridline, i and j are gridline indices. The value of a_0 through a_5 and b_0 through b_5 are the real and apparent coordinate parameters that are fitted by polynomial function. In addition to the correction given above, the unknown real coordinate located in between other known coordinates ((x_i, x_{i+1}) and (y_j, y_{j+1})) is evaluated by using bilinear-interpolation method as

$$\begin{aligned} x', y' = \quad & (x_i, y_j).\frac{\{(u_{i+1}-u).(v_{j+1}-v)\}}{(u_{i+1}-u_i).(v_{j+1}-y_j)} + (x_{i+1}, y_j).\frac{\{-(u_m-u).(v_{j+1}-v)\}}{(u_{i+1}-u_i).(v_{j+1}-y_j)} + \\ & (x_i, y_{j+1}).\frac{\{(u_{i+1}-u).-(v_j-v)\}}{(u_{i+1}-u_i).(v_{j+1}-y_j)} + (x_{i+1}, y_{j+1})\frac{\{-(u_i-u).-(v_j-v)\}}{(u_{i+1}-u_i).(v_{j+1}-y_j)} \end{aligned} \quad (3)$$

where, x' and y' are the real coordinates located in between other known coordinates in horizontal and vertical directions, respectively.

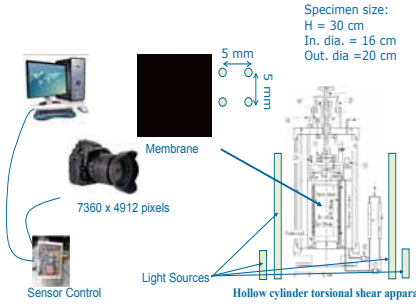

Fig. 5: Configuration of photo control system

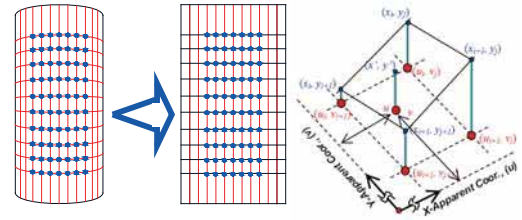

Fig. 6: Illustration of image correction

Strain was calculated from displacement vector and defined by the shape function matrix and the displacement matrix of the four nodes as with finite element analysis. In this research, strain was calculated at the center of each element. The contours were depicted on the basis of this strain. A linear interpolation method is employed to make contour plots of strains.

TEST RESULT AND DISCUSSION

In order to investigate the behavior of segregated Katori sand, drained monotonic loading and undrained cyclic loading are applied.

1. Drained Monotonic Loading Test

Figure 7 shows the relationships between the shear stress ratio (τ/p') and the global shear strain (γ_G), and Fig. 8 shows the contour plots of the local volumetric strain and local shear strain evaluated at prescribed global shear strain values (γ_G = 2.5%, 5.0%, 7.5%, 10%, 15%, and 20%). A positive sign for local volumetric strain represents expansion and a negative sign represents compression.

Yoshida et al. (1994) reported formation of shear strain localization is initiated at the states when the mobilized strength of geomaterial reaches peak stress (i.e, at γ_G = 10% in the present test). However, in segregation specimen, concentration of local shear strain at the interface between silt layer and sand layer was initiated earlier at γ_G = 2.5% (Fig. 9(a)) and that of local shear strain in sand layer were initiated after γ_G exceeds 10% (Fig. 9(d)). Furthermore, shear strain localization at the interface layer and the sand layer continued to develop until γ_G reaches 20%.

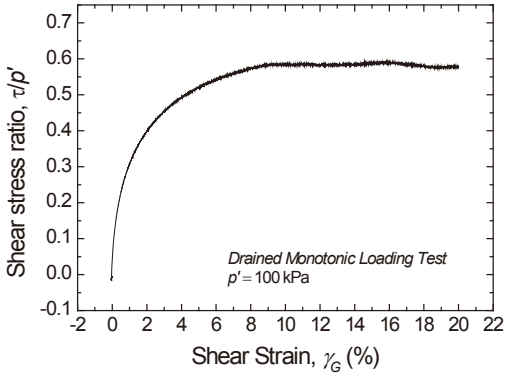

Fig. 7 Shear stress-strain relationship

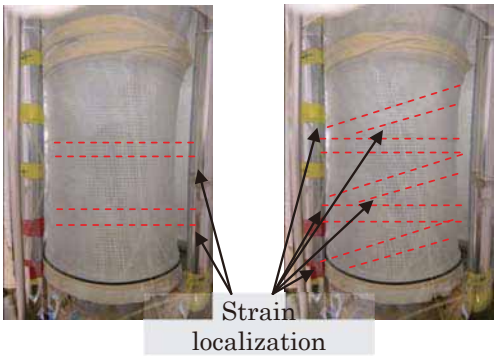

(a) 10% (b) 20%

Fig. 8 Specimen photos at γ_G = 10% and 20%

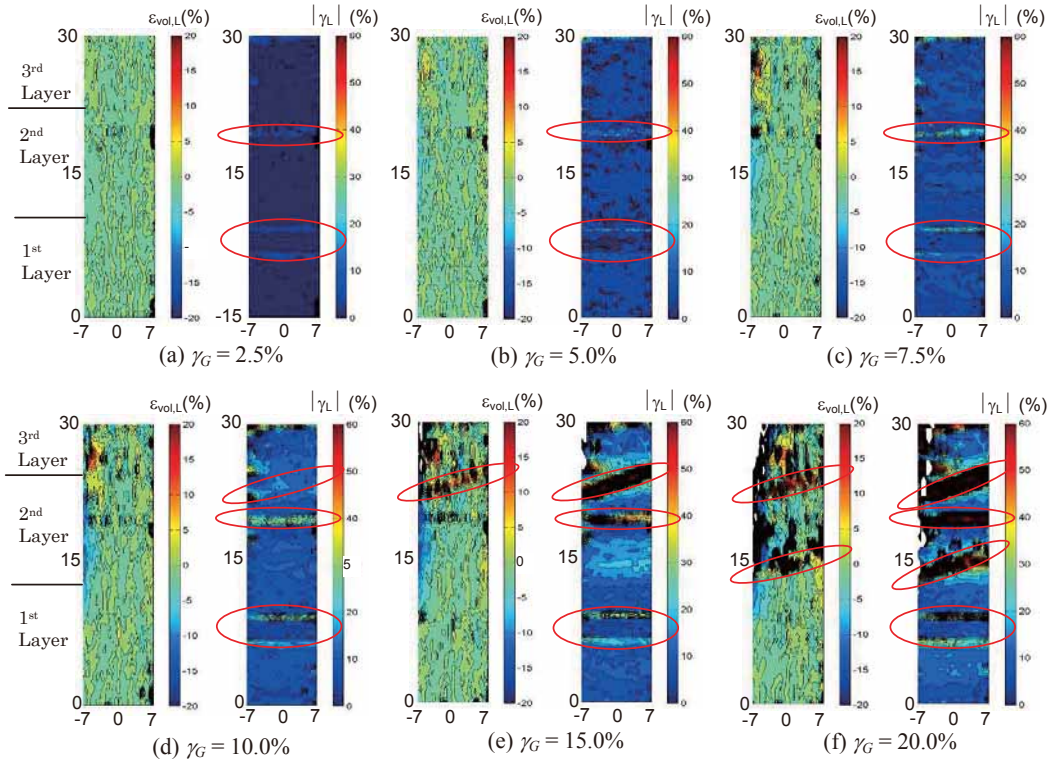

(a) γ_G = 2.5% (b) γ_G = 5.0% (c) γ_G =7.5%

(d) γ_G = 10.0% (e) γ_G = 15.0% (f) γ_G = 20.0%

Fig. 9: Local strain plot for drained monotonic loading test

In order to understand shear strain localization characteristics, shear band is presented in the form of relationship between the shear displacements across the shear band (*Us*) and shear band expansion is defined as the change of the shear band thickness (*Un*) which is similar to the one used by Yoshida et al., 1994 and Wahyudi, 2011. Shear displacement and shear band expansion in the post-peak stress state presented as $Us^* = Us - Us_{peak}$ and $Un^* = Un - Un_{peak}$, respectively, where Us_{peak} and Un_{peak} are the values of *Us* and *Un* at the peak stress state. Fig. 10 shows the relationship between shear displacement and shear band expansion for sand part and silt part at third layer. In Fig. 10(a), each

pairs of observation points at sand part of strain localization show dilative behavior with peak expansion, Un_{max} = 0.37 cm indicate by arrow in Fig. 10(a). However, Fig. 10(b) shows that silt part of strain localization behaves differently, and on the average value, it shows compressive to dilative with peak expansion, Un_{min} = - 0.06 cm. In the post-peak shear displacement and shear band expansion relationship shown in Fig. 11, the sand layer shows dilative behavior and silt layer ($Us_{peak(average)}$ = 0.29 cm , $Un_{peak(average)}$ = 0.079 cm), in average value, shows dilative behavior. However, in each pairs of observation points, silt layer behavior is still unclear ($Us_{peak(average)}$ = 0.28cm, $Un_{peak(average)}$ = -0.027cm).

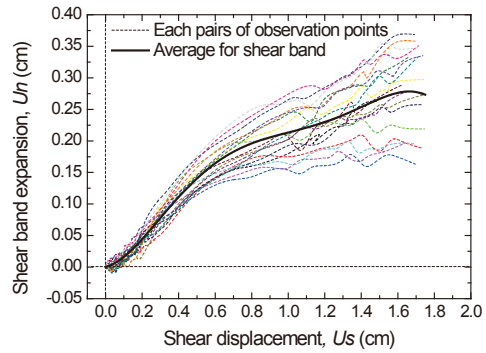

Fig. 10(a): Shear band expansion-shear displacement relationship in sand layer

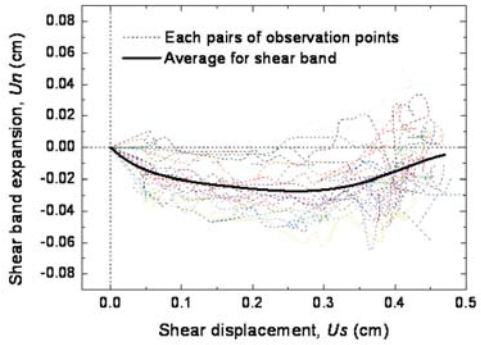

Fig. 10(b): Shear band expansion-shear displacement relationship in silt layer

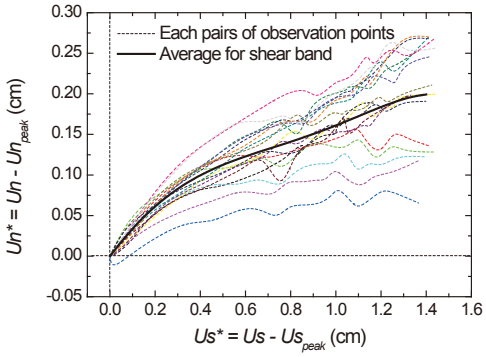

Fig. 11(a): Post-peak shear band expansion- post peak shear displacement relationship in sand layer

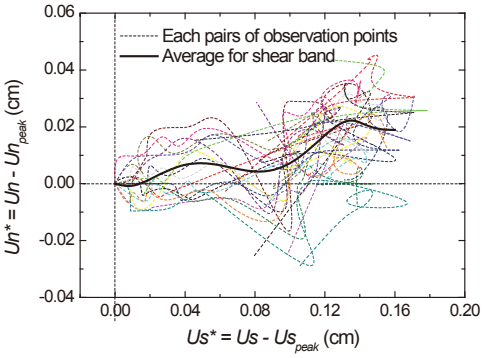

Fig. 11(b): Post-peak shear band expansion- post peak shear displacement relationship in silt layer

2. Undrained Cyclic Loading Test

The effective stress path and stress-strain relationship are shown in Fig. 12 and Fig. 13 for CSR = 0.10, Fig. 15 and Fig. 16 for CSR = 0.15, and Fig. 18 and 19 for CSR = 0.20. The numbers 1, 2, 3, and 4 in these figures correspond to the stages where the contour plots of local shear strain were made as shown in Fig. 14, Fig. 17, and Fig. 20. Diagonal line patterns of high concentration of local shear strains in these figures are affected by the membrane wrinkled. The membrane wrinkle was developed when the torsional loading reversed after reach maximum amplitude of shear stress.

For the test with CSR = 0.10, the global shear strain amplitude starts to increase drastically after 159 cycles, in the same manner as uniform loose sand. However, the local deformation of specimen does not start uniformly but starts gradually. That is due possibly to the effect of silt layer as we can see more clearly in Fig. 14. The specimen deformation starts from the first layer (Stage-2) at τ = -10 kPa and γ_G = -4.5%, then the second layer (Stage-3) at τ = 10 kPa and γ_G = 6.9%, and finally the third layer (Stage-4) at τ = -2.3 kPa and γ_G = -9.7%. The distributions of average local shear strain for each stage are shown in Fig. 14 (e). In the interface layer between first layer and second layer, and second

layer and third layer, higher concentration of local shear strain is observed. These concentrations appeared when the effective stress reduced close to zero. This behavior may be caused by a formation of water film when liquefaction happens.

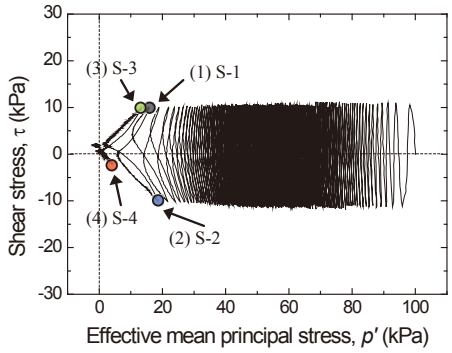

Fig. 12: Effective stress path for CSR = 0.10

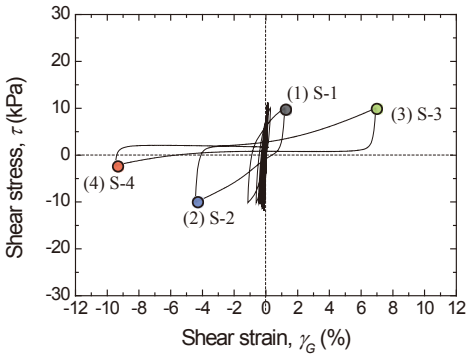

Fig. 13: Shear stress-strain relationship for CSR = 0.10

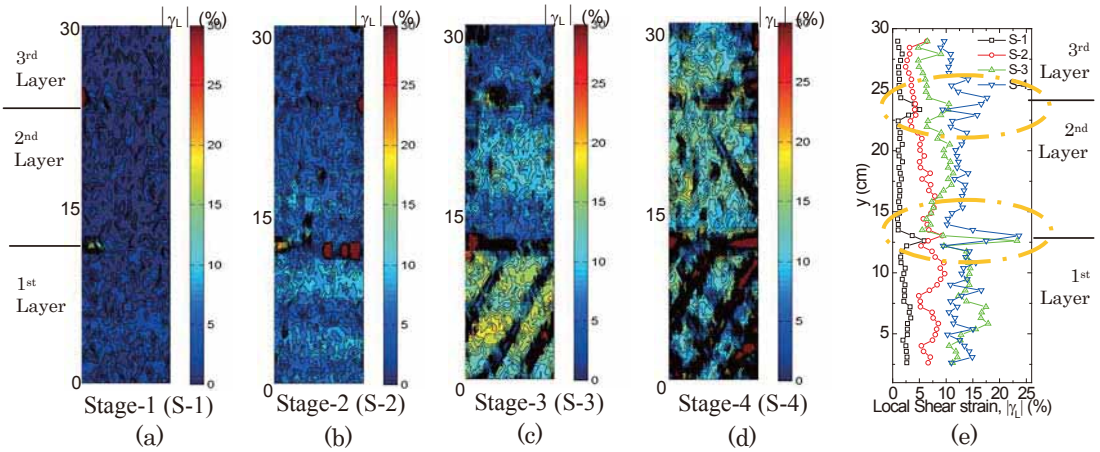

Fig. 14: Local strain plot for undrained cyclic loading test for CSR = 0.10

In another test with CSR = 0.15, the local deformation of specimen also does not start uniformly but starts gradually (Fig. 17). The specimen deformation starts from the second layer (Stage-3) at τ = -15 kPa and γ_G = -8.3%. The distributions of average local shear strain for each stage are shown in Fig. 17 (e), where higher concentration of local shear strain is also observed in the interface layer.

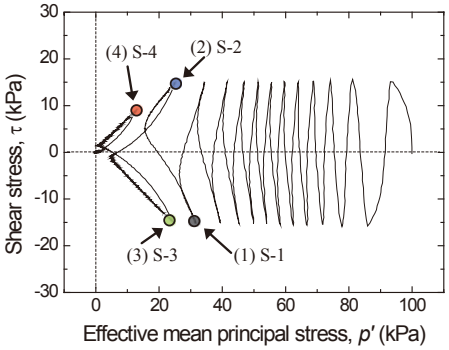

Fig. 15: Effective stress path for CSR = 0.15

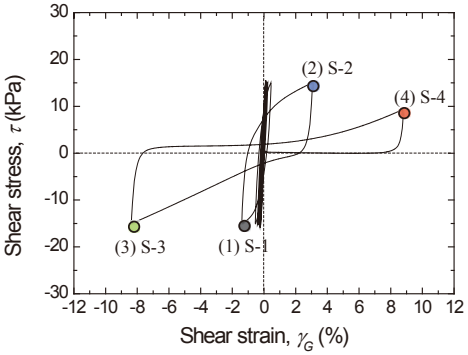

Fig. 16: Shear stress-strain relationship for CSR = 0.15

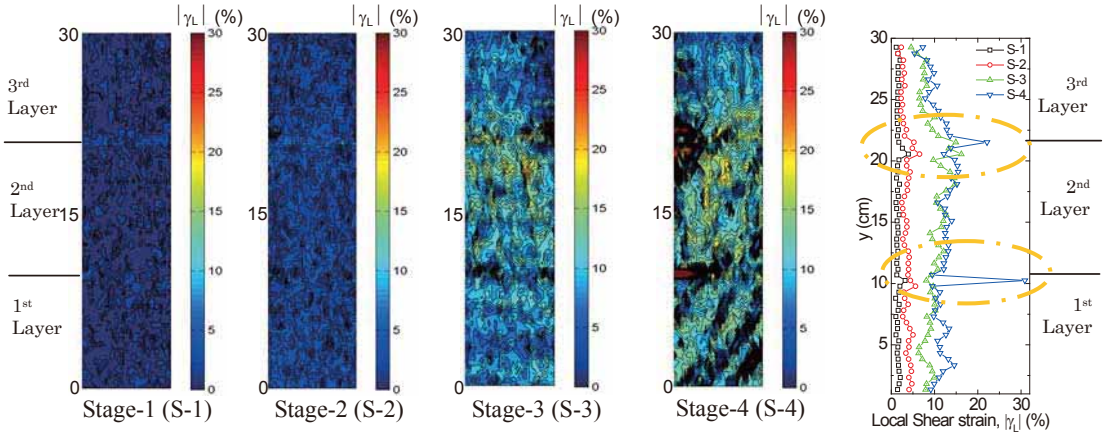

Fig. 17: Local strain plot for undrained cyclic loading test for CSR = 0.15

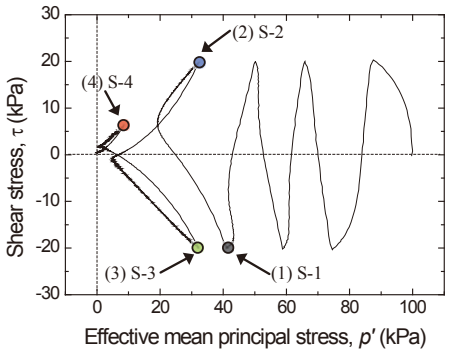

Fig. 18: Effective stress path for CSR = 0.20

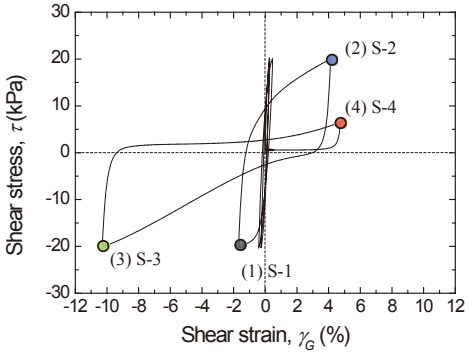

Fig. 19: Shear stress-strain relationship for CSR = 0.15

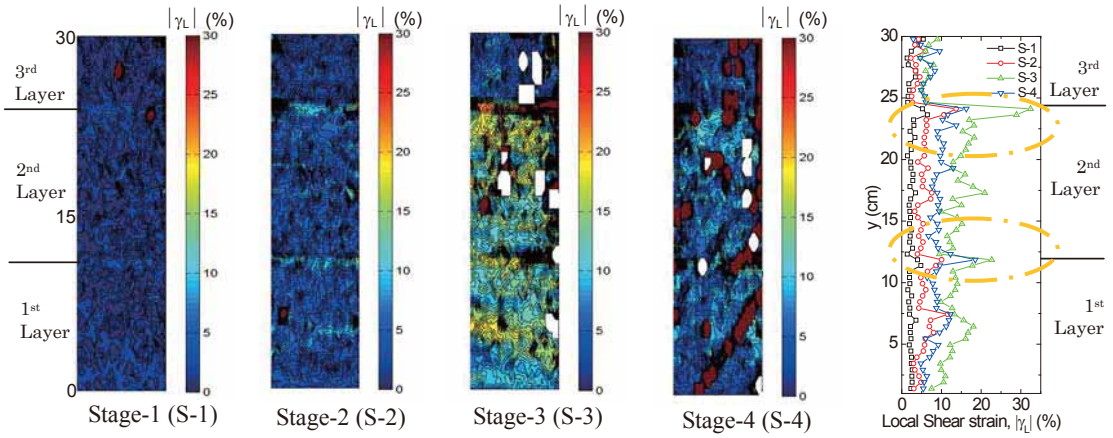

Fig. 20: Local strain plot for undrained cyclic loading test for CSR = 0.20

The test results with CSR = 0.20 (Fig. 20) also support that the local deformation of specimen does not start uniformly. The specimen deformation starts from the first layer and second layer (Stage-3) at τ = -20 kPa and γ_G = -10.2%. Higher concentration of local shear strain is also observed in the interface layer.

CONCLUSION

The soil specimens were reconstituted by depositing Katori sand particles in the acrylic pipe through water sedimentation, resulting into segregation, forming a silt layer at the top of specimen. The local deformation of segregated specimen of Katori sand are investigated by special image analysis technique for both drained monotonic loading test and undrained cyclic loading test. From the test results, it was observed in drained monotonic loading test, formation of shear band was initiated at interface layers before the shear stress reached its peak value. Shear band in sand layers shown positive dilatancy. However, shear band in silt layers is still unclear. For undrained cyclic loading test, the specimen deformed gradually, where accumulation of local shear strains start order are random can be from first layer, second layer or third layer. During undrained cyclic loading test, water film formations are observed in the interface layer.

There are still many behaviors that remain unclear, such as dilatancy characteristic of silt layer, differences liquefaction resistance of uniform and segregated specimen, effect of confining stress, and re-liquefaction resistance. These local deformation properties of segregated specimen observation will contribute to investigate interaction between sand layer and silt layer.

ACKNOWLEDGMENT

The authors wish to express their sincerest gratitude to Mrs. Yukika Miyahita, Mr. Seto Wahyudi, and Mr. Takeshi Sato for their highly cooperative supports made during the development of image analysis technique and during the assembling works of both the mechanical and electronic components of the testing apparatus.

REFERENCES

Alshibli, K. A. and Sture, S. (1999). “Sand shear band thickness measurements by digital imaging techniques.” *Jounal of Comp. in Civil Eng.*, 13(2), 103 – 109.

Brennan, A.J. and Madabhushi, S. P. G. (2005): “Liquefaction and Drainage in Stratified Soil”. *Journal of Geotechnical and Geoenvironmental Engineering*, Vol. 131(7). ASCE.

Desrues, J., Lanier, J., and Stutz, P. (1985). “Localization of the deformation in tests on sand sample.” *Engrg. Fracture Mech.*, 21(4), 909 – 921.

Desrues, J., Chambon, R., Mokni, M., and Mozerolle, F. (1996). “Void ratio evolution inside shear bands in triaxial sand specimens studied by computed tomography.” *Geotechnique*, London, (3), 539 – 546.

Desrues, J. and Viggiani, G. (2004), “Strain localization in sand: an overview of the experimental results obtained in Grenoble using sterophotogrammetry,” *Int. J. Numer. Anal. Meth. Geomech*, Vol. 28, pp. 279-321. (N.R.)

Fauzi, U.J. and Koseki, J. (2013): “Feasibility of segregated sample preparation using water sedimentation.” *Proceeding of 15th International JSCE Summer Symposium*.

Harris, W. W., Viggiani, G., Mooney, M. A. and Finno, R. J., (1995), “Use of stereophotogrammetry to analyze the development of shear bands in sand,” *Geotechnical Testing Journal*, Vol. 28, No. 4, pp. 405-420. (N.R) – Not in UT

Miura, S., and Toki, S. (1982): “A sample preparation method and its effect on static and cyclic deformation-strength properties of sand.” *Soils and Foundations*, 22(1), pp. 61–77.

Kokusho, T., Watanabe, K. and Sawano, T. (1998): “Effect of water film on lateral flow failure of

liquefied sand." *Proceedings of the 11th European Conference on Earthquake Engineering (Paris)*, CD publication, ECEE/T2/kokeow.pdf.

Kokusho, T. (2000): "Mechanism for water film generation and lateral flow in liquefied sand layer." Soils and Foundation, 40(5), pp.99–111.

Lin, H. and Penumadu, D. (2006) "Strain localization in combined axial-torsional testing on kaolin clay." *Journal of Mech. Eng.*, (N.R.)

Rechenmacher, A. L. (2003). "Imaging-based experimental soil mechanics," *Proceedings of the 1st Japan – US Workshop on Testing, Modelling and Simulation*, No. 156, pp. 653-663. (N.R.)

Seed, H.B. (1987): "Design problems in soil liquefaction." *Journal of Geotechnical Engineering*, 113(8). ASCE.

Sutton, M. A., McNeill S. R., Helm J. D., and Chao Y. J. (1983) "Advances in two-dimensional and three-dimensional computer vision," *Image and Vision Computing*, Vol. 1, No. 3, pp. 133-139. (N.R)

Tatsuoka, F., Ochi, K., Fujii, S., and Okamoto, M. (1986): "Cyclic undrained triaxial and torsional shear strength of sands for different sample preparation methods." *Soils and Foundations*, 26(3).

Wood, M., Yamamuro, J.A., Lade, P.V. (2008): "Effect of depositional method on the undrained response of silty sand." *Canadian Geotechnical Journal*, 45(11): 1525-1537.

Wahyudi, S., Miyashita, Y., Koseki, J. (2011): "Shear Band Behavior of Sand in Torsional Shear Tests by Means of Image Analysis." *Proceeding of 13th International JSCE Summer Symposium*.

Yoshida, T., Tatsuoka, F., M. S. A. Siddiquee, Kamegai, Y. and C. S. Park (1994): "Shear banding in sands observed in plane strain compression." *In R Chambon, J Desrues, I. Vardoulakis (eds). Localization and Bifurcation Theory for Soils and Rocks*: 165 – 179. Balkema: Rotterdam.

Yoshimine, M. and Koike, R. (2005). Liquefaction of clean sand with stratified structure due to segregation of particle size, *Soils and Foundation*, 45 (4), pp. 89-98.